Fluorescence and Optical Maser Effects in $CaF_2:Sm^{++}$

W. KAISER, C. G. B. GARRETT, AND D. L. WOOD
Bell Telephone Laboratories, Inc., Murray Hill, New Jersey
(Received March 17, 1961)

Measurements are reported of absorption, emission, and activation spectra in $CaF_2:Sm^{++}$, and also of fluorescence lifetime. A revised level scheme is proposed. Observations of optical maser effects were made at liquid hydrogen and liquid helium temperatures over a wide range of pumping intensities. For illumination in the 6400-A band, the threshold intensity of illumination was about 20 w cm^{-2}. Observations are reported of the dependence of the intensity of the maser beam on the pumping intensity. Photographic observations, made both with or without a Fabry-Perot etalon, show that on one particular sample five distinct frequencies were present in the maser signal, and that the number of modes excited was of the order of 1000.

INTRODUCTION

FOR the past year we have been investigating fluorescence associated with rare-earth ions in calcium fluoride and similar crystals. Considerable interest at the present time attaches to certain phenomena which can occur at very high excitation levels in such materials; in particular, the optical maser effect. On the basis of previously published information,[1] it has been suspected for some time that one particularly favorable system for the observation of optical maser effects is $CaF_2:Sm^{++}$. Recently Sorokin and Stevenson have indeed reported the operation of a $CaF_2:Sm^{++}$ optical maser.[2] In this paper, we shall present the results of more detailed spectroscopic and optical maser experiments with this material. Specifically, we shall present: (i) an amended level scheme for the Sm^{++} ion, with an attempt at some term assignments; (ii) observations of the distribution of the energy in the emitted light over wavelength, and of the width of the principal emission line, as functions of temperature; (iii) a confirmation of the previously reported fluorescence lifetime; (iv) a determination of the quantum efficiency as a function of the exciting wavelength; (v) a measurement of the threshold intensity of illumination for the onset of optical maser action in several samples having the parallel-reflector geometry; (vi) a study of the dependence of maser output on pumping level, and of the lateral fluorescence in the region beyond the maser threshold; and (vii) an examination of the directionality and of the frequency distribution in the maser beam by means of a Fabry-Perot etalon.

Most of the crystals studied were grown by H. Guggenheim of Bell Telephone Laboratories.[3] The crystals were doped with samarium in the range 0.02 to 1% per mole. Reducing conditions during growth are required in order to encourage the divalent rather than the trivalent form of the samarium; the difference between the two is at once obvious to the eye, since $CaF_2:Sm^{++}$ has an intense green color, even at quite low concentrations, while $CaF_2:Sm^{3+}$ appears to the eye to be transparent. Generally, our crystals were considerably darker in color than others having the same nominal samarium concentration obtained elsewhere; even so, during our investigation it transpired that even in the darkest crystals much of the samarium was still in the trivalent state.

The paper is divided into two parts: part A, concerned with the (linear) fluorescence processes and part B, dealing with the optical maser effects.

A. FLUORESCENCE PROPERTIES

1. Absorption and Emission Spectra

The measurements to be reported in this section were made on a sample with a total samarium content of 0.05 mole percent. From reasoning to be given in Sec. A.4 it is estimated that approximately 20% of the samarium was present in the divalent state, and the rest in the trivalent state. Thus the concentration of Sm^{++} is approximately 3×10^{18} atoms cm^{-3}.

Measurements of absorption and emission spectra were made at a number of temperatures between room temperature and the liquid helium range. Measurements of absorption were made with a Cary model 14 spectrophotometer. In addition, measurements of absorption and emission in the vicinity of the main emission line (at 14 497 cm^{-1}) were made under higher resolution with a Bausch & Lomb dual grating spectrograph at dispersions of about 8 or 1.6 A/mm. For the emission measurements, the fluorescence was excited with a tungsten filament lamp.

The broad outline of the room temperature absorption spectrum is given in Fig. 1 and clearly shows the conspicuous broad absorption bands near 23 500 cm^{-1} and 16 000 cm^{-1} characteristic of Sm^{++}. As the temperature is lowered, considerable fine structure in these bands appears; at liquid helium temperatures, the bands are partially resolved into many components of various intensities and linewidths. Also to be seen in Fig. 1, in the curve for 1.8°K, are sharp absorption lines at 25 132 cm^{-1}, 25 081 cm^{-1}, and 24 987 cm^{-1}. These correspond with known absorptions for the trivalent ion Sm^{3+}. The other conspicuous feature of Fig. 1 is a set of sharp absorption lines between 14 000 and 15 000 cm^{-1}, to which we shall return in a moment.

[1] P. P. Feofilov, Zapiski Vsesoyuz Mineral Obschestva **85**, 569 (1956); Optika i Spektroskopiya **1**, 992 (1956).
[2] P. P. Sorokin and M. J. Stevenson, IBM J. Research and Develop. **5**, 56 (1961).
[3] H. Guggenheim, J. Appl. Phys. **32**, 1337 (1961).

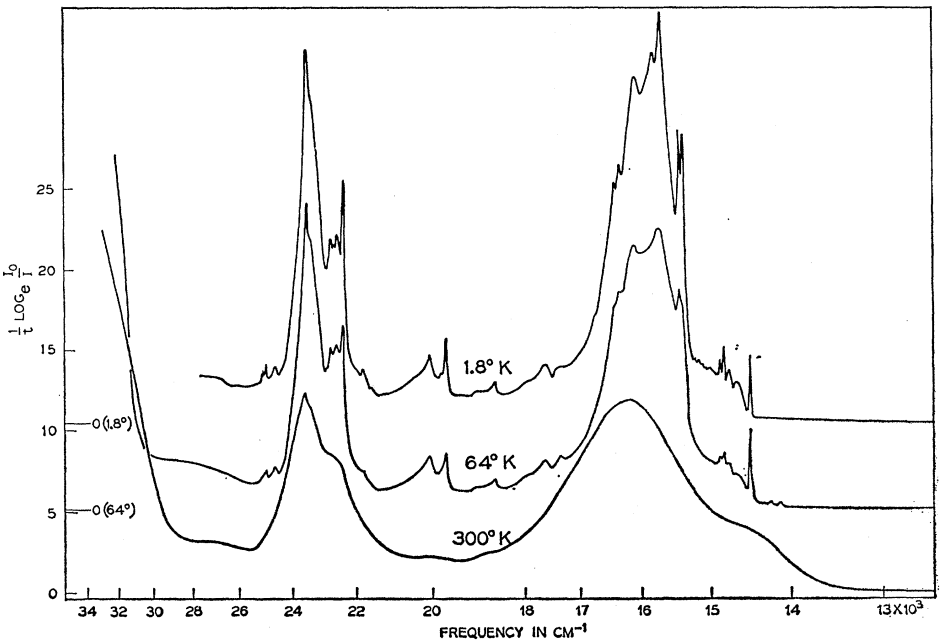

FIG. 1. Absorption spectrum for 0.05% Sm (0.01% Sm^{++}) in calcium fluoride.

Absorption measurements have also been made in the infrared. The results, which are not shown in Fig. 1, are as follows. Groups of weak lines occur at 9260 cm^{-1}, 8130 cm^{-1}, 7246 cm^{-1} and 6896 cm^{-1}; these lines are also found in samples of calcium fluoride containing samarium grown in an oxidizing environment, which lack the strong absorption bands characteristic of Sm^{++}, and may be assigned to Sm^{3+}. In some samples, made under conditions in which forming gas (N_2+H_2) had been added to the gaseous ambient to promote the appearance of divalent samarium, there are lines or bands in the region around 2100 cm^{-1} or 3000 cm^{-1}, which are due to C≡N and C−H molecular groupings, respectively.

The only feature in the infrared part of the absorption spectrum which can probably be ascribed to Sm^{++} is a line at 963 cm^{-1}.

The portion of the absorption spectrum in the range 14 000–15 000 cm^{-1} is shown in greater detail in Fig. 2. Absorption lines are visible at about 14 128 cm^{-1} and 14 241 cm^{-1}; a much stronger line at 14 497 cm^{-1} is off scale at the left-hand side of the figure. Figure 3 shows

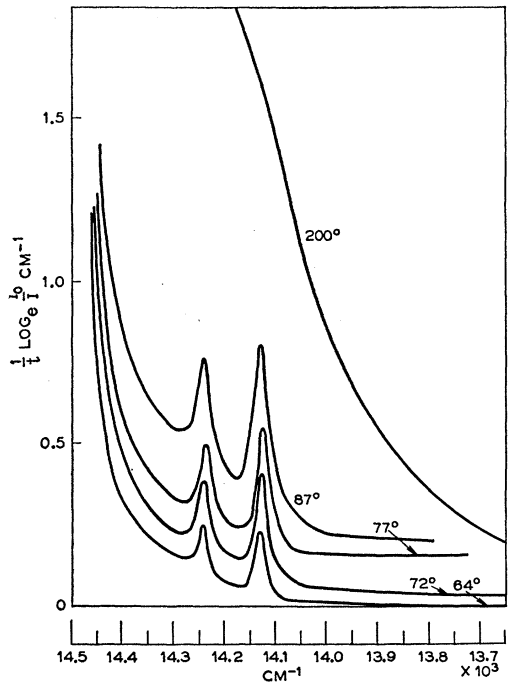

FIG. 2. Detail of absorption spectrum.

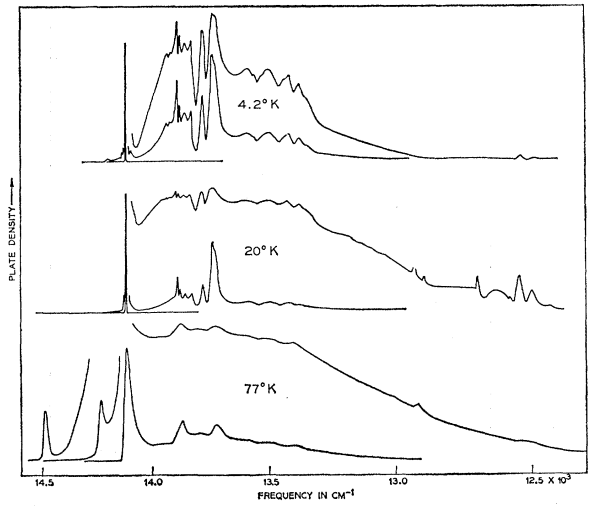

FIG. 3. Fluorescence emission spectrum for 0.05% Sm (0.01% Sm^{++}) in calcium fluoride. The ordinate represents plate density.

the emission spectrum in this region, as obtained by microphotometer traces of plates obtained with the Bausch & Lomb instrument. Conspicuous emission lines occur at 14 120 cm^{-1}, 14 230 cm^{-1}, and 14 497 cm^{-1}. Small shifts in the positions of the emission and absorption lines occur when the temperature is changed; careful measurement shows, however, that at any one temperature the three emission lines coincide with the three absorption lines within the accuracy of the measurements.

We shall postpone for the moment the discussion of the absolute strengths of the absorption and emission lines, which will be the subjects of later sections. It is convenient to discuss here, however, the temperature dependence of the principal absorption and emission lines. At liquid helium temperatures the only absorption line remaining is that at 14 497 cm^{-1}, and the only emission line is that at 14 118 cm^{-1}. As the temperature is raised to some value in the vicinity of 50°K, the absorption lines at 14 230 cm^{-1} and 14 118 cm^{-1} make their appearance, and at some point in the same range of temperature the remaining two emission lines also appear. If the temperature is raised beyond 80–90°K, the 14 497-cm^{-1} absorption line becomes noticeably weaker, while the other two absorption lines continue to become more enhanced. Finally at some temperature in the vicinity of 130°K all of the absorption and emission lines become submerged in the tail of the broad absorption band centering around 16 000 cm^{-1}, which at these temperatures begins to extend into the region under discussion.

To investigate quantitatively the temperature dependence of the 14 118 cm^{-1} and 14 230 cm^{-1} absorption lines, measurements of the area $\int K d\nu$ under the absorption line were made as a function of temperature and the results plotted logarithmically against $1/T$ (Fig. 4). The slopes of both curves are the same, within the accuracy of the experiments, and a nominal value of -240°K for the slope is obtained. This slope which is equal to E/k in the Boltzmann function $e^{-E/kT}$ corresponds to an energy separation of $E=170$ cm^{-1}. However, several factors in our experiments operate to decrease the slope of $\int K d\nu$ vs $1/T$ and increase the apparent energy separation of the ground and first excited levels. These are: (1) More than one excited level is being populated, especially at higher temperatures. (2) The ground level will tend to be depleted at higher temperatures. (3) Appreciable internal heating in the sample from absorption of the measuring radiation may occur, especially at low temperatures where heat capacity of CaF_2 is small. (4) As the temperature decreases, the linewidth decreases, and for the transitions involved the instrumental resolving power may be inadequate to record the true linewidth. Thus the measured intensity will decrease more slowly with temperature. We believe that all these factors could produce a slope which is as much as 50% too small, and that the energy separation for the levels involved may be as large as 263 cm^{-1} (see Sec. A.4).

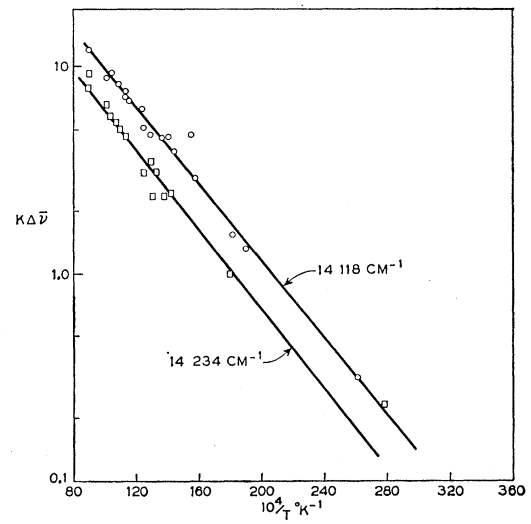

FIG. 4. Plot of the quantity $\int K d\nu$ against the reciprocal of the absolute temperature for the 14 118-cm^{-1} and 14 234-cm^{-1} absorption lines. K is in cm^{-1} and ν in wave-number units (cm^{-1}). (Legend of ordinate should read $\int K d\nu$.)

Results of comparable accuracy for the temperature dependence of the 14 230 cm^{-1} and 14 497 cm^{-1} emission lines have not yet been obtained, but the strengths of these lines relative to the 14 118 cm^{-1} line are found to be 0.063 and 0.0017, respectively, at 77°K.

Measurements of the width of the 14 118 cm^{-1} emission line as a function of temperature were made by photographing the emission spectrum at a number of different exposure times, making microdensitometer traces of the line contours, and correcting for the emulsion characteristic by use of a previously determined plate calibration curve. Results are given in Table I.

One other feature of the emission spectrum is noteworthy. This is the appearance of a broad continuous emission extending from the sharp line at 14 118 cm^{-1} to a limit some 1000 cm^{-1} lower in frequency. To estimate the ratio of the energy radiated in this continuum to that contained in the principal emission line at 14 118 cm^{-1}, we have compared the areas under the appropriate microphotometer traces similar to those shown in Fig. 3. We find that at 77°K the continuum contains about 10 times as much energy as the sharp line; at 20°K the ratio has fallen to 5, and at 4.2°K to 3.5.

2. Activation Spectrum

Qualitatively, the "activation spectrum" of a fluorescent material means a plot of the brightness of the fluorescence as a function of the wavelength of the exciting light. This brightness, of course, depends on the intensity of the exciting light, the absorption constant at the wavelength in question, the quantum efficiency, and the geometry of the experiment. By making measure-

ments on parallel-sided slabs, illuminated in some defined way with a known intensity of illumination, it is possible to sort these various factors out. A detailed discussion of the techniques used will be given in a subsequent paper. In presenting the results obtained with $CaF_2:Sm^{++}$, we shall define two quantities: (i) *The quantum efficiency per absorbed photon* (η)*:* the ratio of the rate of emission of photons of fluorescent light to the rate of absorption of photons of wavelength λ. (ii) *The quantum efficiency per incident photon* (η^*)*:* the ratio of the rate of emission of photons of fluorescent light to the rate of arrival (at or close to normal incidence) of photons of wavelength λ.

The true quantum efficiency, of course, is η. The quantity η^* is related to η through the fractional absorbance of the parallel-sided slab, and consequently depends on the thickness of the slab. An "activation spectrum" is then a plot, for some particular thickness, of η^* against λ.

Figure 5 shows an activation spectrum for a $CaF_2:Sm^{++}$ sample 0.32 cm thick, having a total samarium content of 0.05%. The measurements were made at liquid nitrogen temperatures, and count *all* the

TABLE I. Linewidth as function of temperature.

Temperature (°K)	Line frequency ν (cm^{-1})	Wavelength (A)	Half-peak width (cm^{-1})
77	14 118	7083	30.4
64	14 118	7083	14.6
20	14 114	7085	1.6
4.2	14 114	7085	1.3

emitted fluorescent light, including the long-wavelength continuum. It will be seen that η^* has peaks at wavelengths corresponding to the absorption maxima of Fig. 1. Making use of the absorption data, it is found that the true quantum efficiency η is 1.3 (with an uncertainty of a factor of about 1.5) for *all* wavelengths between 3000 and 6600 A. This remarkable result shows that all of the bands are equally effective in populating the initial states for the fluorescent emission.

Since only about 10% of the fluorescent emission at 77°K is in the strongest sharp line, the quantum efficiency for emission in this line is only about 0.1. Measurements of activation spectra have not been made at lower temperatures, but we have some evidence that the total fluorescent emission remains unchanged. This means, for example, that at 20°K the quantum efficiency for emission into the 14 118-cm^{-1} line will have risen to 0.2.

3. Fluorescent Lifetime

The decay time of the 14 118-cm^{-1} emission line at 20°K was determined using an experimental arrangement similar to that to be described in part B. The sample was excited by an FX 12 capillary flashlamp,

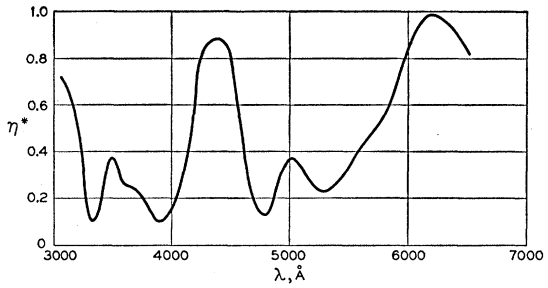

FIG. 5. Activation spectrum for 0.05% Sm (0.01% Sm^{++}). The figure shows η^*, the quantum efficiency per incident photon, for a slice 0.32 cm thick. $T=77°K$.

discharging a circuit giving a lamp decay time of 2×10^{-7} sec. The time constant of the detector was smaller than 10^{-7} sec. The fluorescence decay was followed over 8×10^{-6} sec and showed no departure from the simple exponential form. The lifetime τ was found to be 2×10^{-6} sec, with an uncertainty of about 10%; this compares with Feofilov's value of 1.4×10^{-6} sec.

4. Interpretation

Let us now turn to the interpretation of the foregoing data. Previously published experimental and theoretical results on the spectroscopy of Sm^{++} are meager. Feofilov[1] has proposed a level scheme, but has made no term assignments. Butement[4] has attempted to assign the lowest lying levels, on the basis of absorption and fluorescence measurements on $BaCl_2:Sm^{++}$.

Butement's scheme is based on the supposition that, since Sm^{++} is isoelectronic with Eu^{3+}, the lowest levels should consist, as they certainly do in Eu^{3+}, of the successive components of a normal ^7F multiplet. Taking the ground state as $^7F_0$, Butement locates from the fluorescence the $^7F_1$ at 269 cm^{-1}, the $^7F_2$ at 834 cm^{-1}, the $^7F_3$ at 1493 cm^{-1}, and the $^7F_4$ at 2296 cm^{-1}. In a suitably transparent host lattice, the existence of these levels should lead to fairly sharp absorption lines or groups of lines at the wave-number values indicated. In CaF_2, however, the first lies within the region of strong host lattice absorption. The absorption at 963 cm^{-1} mentioned in Sec. A.1 might be associated with the $^7F_0 \rightarrow {}^7F_2$; the others, for some reason, have not been observed.

Turning next to the group of absorption and emission lines around 14 000 cm^{-1}, we note that Feofilov's analysis is based on his conclusion that the 14 497-cm^{-1} line is a "resonance" line. This leads Feofilov to identify the final state of the 14 497-cm^{-1} absorption with the initial state of the 14 118-cm^{-1} emission line, and therefore to locate the final state of the emission line 379 cm^{-1} (or 396 cm^{-1}, according to his measurements) above the ground state. According to the results reported in Sec. A.1, however, the 14 497-cm^{-1} line is *not* a resonance line, since the emission at this frequency vanishes

[4] F. D. S. Butement, Trans. Faraday Soc. 44, 617 (1948).

at low temperatures. From the temperature-dependence of the *absorption* lines at 14 118 and 14 230 cm^{-1}, we may conclude, although with some reservation, that the lower states for these transitions lie 263 cm^{-1} above the ground state. This means that the upper state for the 14 230-cm^{-1} transition lies, within the experimental accuracy, at the same energy as the upper state of the 14 497-cm^{-1} transition, and may therefore be identified with it. On this basis we may then construct the level scheme shown in Fig. 6.

Next we shall attempt to calculate the oscillator strengths for the three transitions under discussion. The oscillator strength associated with an absorption line is given by the equation:

$$f=(mc/\pi e^2N)\int K d\nu, \tag{1}$$

where N is the density of atoms in the lower state of the transition. The oscillator strength associated with an emission line, on the other hand, is given by

$$f=mc^3/8\pi^2e^2\nu^2\tau, \tag{2}$$

where τ is the radiative lifetime, which will be equal to the measured lifetime divided by the quantum efficiency for emission into the line in question.

The lines at 14 118 cm^{-1} and 14 234 cm^{-1} originate in absorption from an excited level, and the fraction of Sm^{++} ions excited into the 263 cm^{-1} level is still small at 77°K. For these lines, $N=N_0\exp(-263\ cm^{-1}/kT)=N_0/132$, while we may write $N=N_0$ for the line at 14 497 cm^{-1}, which originated in the ground state. The value of N_0, the total density of Sm^{++} atoms in the crystal, was obtained in the following way. First, the distribution coefficient for Sm in crystals of CaF_2 grown from the melt is very nearly unity.[5] Thus, the total Sm concentration is that which was originally added. Second, the Sm^{++}/Sm^{3+} ratio was determined by converting the Sm^{++} to Sm^{3+} in an oxidizing atmosphere for a sample containing 0.05 mole Sm/mole CaF_2. The increase in absorption at 8152 cm^{-1} where Sm^{3+} absorbs indicated that 20% of the total samarium was in the divalent state. The sample was found in this way to contain 2.6×10^{18} atoms Sm^{++}/cm^3. From Eq. (1) and the values of N just determined, the f numbers for the lines in question are those given in Table II. The f numbers for certain other lines are also given in the table.

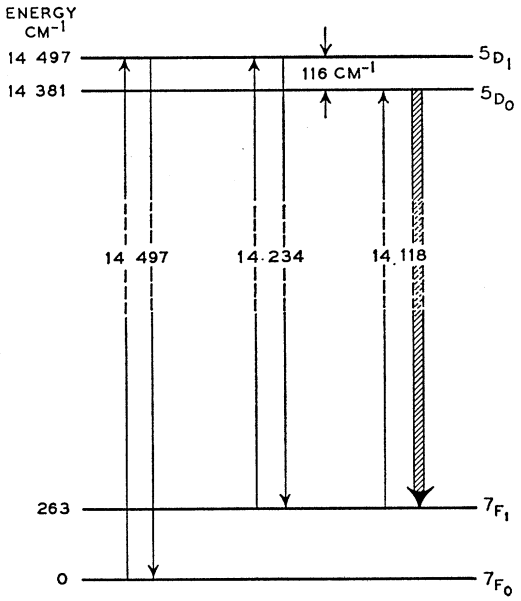

FIG. 6. Level scheme for Sm^{++} in CaF_2.

TABLE II. Absolute intensities of selected absorption lines.

λ (A)	ν (cm^{-1})	$K_{max}=D/t$ (cm^{-1})	$\Delta\nu$ (cm^{-1})	f
7083	14 118	21[a]	30	6.9×10^{-4}
7025	14 234	13.2[a]	27	3.9×10^{-4}
6902	14 497	1.6	20	3.5×10^{-5}
6743	14 830	0.77	20	1.7×10^{-5}
6723	14 874	0.36	30	1.2×10^{-5}
6360	15 723	10.3	160	1.8×10^{-3}
5082	19 677	1.55	78	1.3×10^{-5}
4468	22 381	5.50	303	1.8×10^{-3}
4248	23 540	8.85	330	3.1×10^{-3}
4002	24 987	0.62	48	3.3×10^{-4}

[a] Corrected for Boltzmann population factor for the lower state at 263 cm^{-1}. Data from 77°K. The other measurements were made at 1.8°K on the Cary instrument. Note that the instrumental linewidth was 10–20 cm^{-1}, so that the values for $\Delta\nu$ quoted above for the 14 497-cm^{-1} and 14 830-cm^{-1} lines are not to be interpreted as true linewidths.

By using Eq. (2) the f number for the line at 14 118 cm^{-1} may be obtained using the radiative lifetime from Sec. A.3; namely, $(2\times10^{-6}/0.1)$ sec at 77°K. The value of $f=3.7\times10^{-4}$ thus obtained is in satisfactory agreement with the value 6.9×10^{-4} obtained from absorption.

As an additional check on these calculations, we have used the f values indicated in Table II to compute the relative strengths of the three emission lines at 77°K, allowing for thermal excitation from the metastable state at 14 381 cm^{-1} to the state at 14 497 cm^{-1}. The values computed are 1:0.076:0.0059, as compared with observed values of 1:0.063:0.0017 (see Sec. A.1). The agreement is satisfactory, if it is noted that self-absorption will reduce the ratio for the 14 497-cm^{-1} line but not for the other two.

With respect to the assignment of the levels indicated in Fig. 6, the following remarks may be made. The state at 263 cm^{-1} lies very close to the position of the $^7F_1$ state as proposed by Butement,[4] which in turn is close to that computed from the screening constant. The observation that the state is not split is consistent with the fact that $J=1$ states do not split in a cubic field. In principle it should be possible to check this assignment by finding, from the temperature dependence of the 14 497-cm^{-1} line, whether the 256-cm^{-1} level has the expected statistical weight of 3, but this has not yet been done.

[5] K. Nassau, J. Appl. Phys. (to be published).

In Eu^{3+}, the next higher group of levels is the ^5D multiplet, with $^5D_0$ lying lowest.[6,7] We may therefore tentatively assign the 14 381-cm^{-1} level to $^5D_0$ and the 14 497-cm^{-1} level to $^5D_1$. Supporting evidence for this is to be found in the absence of the $0 \rightarrow 0$ transition, which is forbidden in a cubic field.

With these tentative assignments, we may proceed further and attempt to locate the $^7F_2 \cdots {}^7F_6$ and the $^5D_2$, $^5D_3$, and $^5D_4$ levels. As mentioned above, the $^7F_2$ level may be tentatively located at 963 cm^{-1}. In addition, there are, as will be seen from Figs. 2 and 3, numerous absorption lines lying at energies higher than 14 497 cm^{-1}, which might be associated with the former, and numerous emission lines lying at energies lower than 14 118 cm^{-1}, forming part of what we have called the "long-wavelength continuum." The number and complexity of these features has so far frustrated a more complete analysis. Of course, states having $J>1$ split in a cubic field, so that the number of intercombination terms increases rapidly as we ascend within each multiplet.

Finally, there are the broad-band features of the absorption and emission spectra. The f numbers for the broad bands are of the order of 10^{-3}. As pointed out by Feofilov[1] and by Butement,[4] such broad and strong bands cannot arise from transitions wholly within the $4f$ shell; thus we are compelled to associate them with allowed $4f \rightarrow 5d$ transitions. Why these should occur in the visible spectrum instead of in the ultraviolet, where the allowed transitions for Eu^{3+} are found, is not at present understood. The close proximity of these $5d$ levels to the $^5D_0$ and $^5D_1$ states of the $4f$ configuration suggests that the unusually large f numbers for the transitions near 14 500 cm^{-1} arise from interactions in which intensity is "borrowed" from the allowed $4f \rightarrow 5d$ transitions.

An alternative possibility that cannot be entirely ruled out is that the sharp lines at 14 500 cm^{-1} as well as the many components of the group near 15 700 cm^{-1} arise from the multiplet components of the $5d$ level, as split by the crystal field. Butement[4] has pointed out that the parent level may have rather high multiplicity and therefore may give rise to the many levels observed even in a highly symmetrical field. In this case, the $(4f)$ transitions might have their customary f numbers ($\sim 10^{-6}$) and so be too weak to be observed.

As for the broad "long-wavelength continuum" in the emission spectrum, all we can suggest at the moment is that, since this persists to low temperatures, it too must be associated with transitions out of the 14 381-cm^{-1} level. We might tentatively associate these transitions with the existence of many overlapping levels lying within about 1000 cm^{-1} of the ground state. This energy figure is of the right order of magnitude to be ascribed to lattice vibrations.

[6] K. H. Hellwege and H. G. Kahle, Z. Physik **129**, 62 (1951).
[7] J. B. Gruber and J. G. Conway, J. Chem. Phys. **34**, 632 (1961).

B. OPTICAL MASER EFFECTS

1. Experimental Arrangements

Samples of $CaF_2:Sm^{++}$ were cut into cylindrical (3-mm diameter and 20-mm length) shape, with the ends of the cylinders polished flat and parallel to approximately 10 seconds of arc and subsequently silvered.

The sample was mounted at the bottom of a vertical stainless steel tube, mounted inside a Pyrex Dewar, so that the sample was in the unsilvered appendix. Various arrangements were made for illuminating the sample. For illumination by a flash of the order of 1 msec duration, the appendix of the Dewar was inserted into a General Electric FT-524 flash tube. This arrangement, however, has the disadvantage that the intensity of illumination of the sample is difficult to estimate with any accuracy; in addition, the lamp is not designed to be run continuously. Alternatively, a confined source is used, and focused on the sample by means of a number of spherical mirrors, each arranged so that the lamp and the sample are as close as possible to the center of curvature, and so that the sample coincides with the tangential line focus of the source. A typical arrangement is shown in Fig. 7; the spherical mirrors in this setup each had a radius of curvature of 20 cm, and the total solid angle was approximately 3.2 sr. The aberrations were small of the order of the size of the sample. For very short pulses, the source was an Edgerton, Germeshausen, and Grier FX-12, which has a maximum rating of about 4 joules for a pulse of duration $\sim 10^{-6}$ sec. For pulses having durations in the range 10^{-5}–10^{-4}

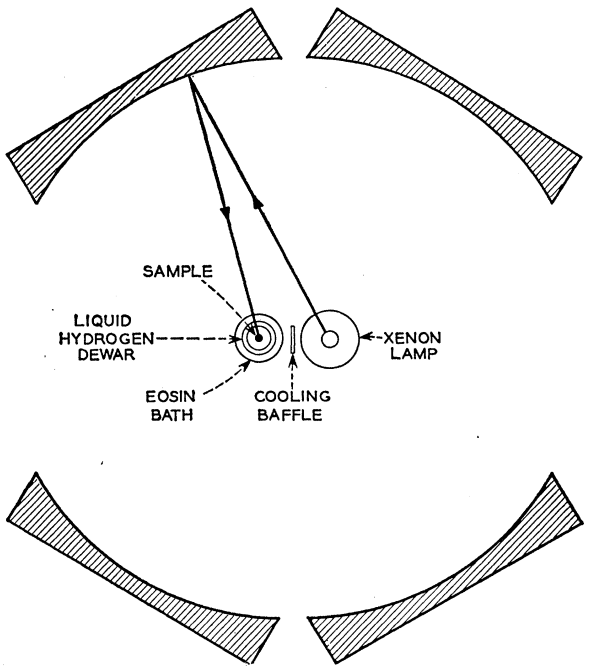

FIG. 7. Arrangement of mirrors for illumination of maser samples with light from a compact arc lamp.

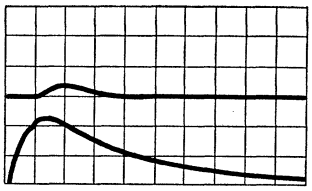

FIG. 8. Optical maser action with a short light flash. Upper beam, maser signal; lower beam, pump signal; time scale, 1 μsec per division. The traces have been smoothed to eliminate electrical pickup from the light circuit.

sec, the source was a Hanovia xenon lamp; this lamp has a rating of 300 joules for pulses of duration $\sim 10^{-4}$ sec, and can also be run up to 30 kw for 0.1 second, or 1 kw continuously. In all cases, selection of the wavelength range of the exciting light was obtained by surrounding the tail of the Dewar with a cellophane filter immersed in water, or by an aqueous solution of suitable transmission properties. In particular, solutions of eosin were found convenient for transmitting light having wavelengths falling within the 16 000-cm^{-1} pumping band.

Arrangements were made for inspecting the light emerging through the end of the sample and up the stainless steel tube, the light emitted from the sides of the sample, and the light from the lamp. To separate the fluorescent light from other wavelengths present, a small spectrometer containing a Bausch & Lomb 1200-line/mm grating was used. Light emerging from the exit slit of this spectrometer was allowed to fall on a 1P-28 photomultiplier, the output of which was displayed on a dual-beam Tektronix oscilloscope. Arrangements were made for displaying simultaneously on the oscilloscope either the lateral fluorescence signal and the lamp intensity, or the maser signal and the lamp intensity.

To investigate the directionality of the maser beam, the light emerging through the end was photographed through a Nikkor 500-mm focal length lens with the film in the focal plane. When, in addition, information on the monochromaticity was required, a 10-mm Hilger Fabry-Perot etalon was set immediately in front of the lens.

Finally, a few measurements were made on the spectral distribution of energy in the light emitted by the lamp. These measurements verified, within the accuracy required for the present investigation, the distribution reported by the manufacturer, and further showed that the distribution was approximately the same when the lamp is operated on a pulse basis.

2. Maser Threshold

The critical excess inverted density for optical maser action is[8]

$$\frac{N}{V} > \frac{8\pi^2 \Delta\nu}{\lambda^2} \frac{(1-R)}{l} \tau, \tag{3}$$

where V is the volume, l the length of the crystal, $\Delta\nu$ the width of the fluorescent line, λ its wavelength, and τ its radiative lifetime, and R is the reflectivity of the ends. If the sides of the sample are illuminated in such a way that the intensity of illumination for wavelengths between λ' and $\lambda'+d\lambda'$ is $I(\lambda')d\lambda$ w cm^{-2}, and if the absorption constant at λ' is $K(\lambda')$ and the quantum efficiency for excitation at that wavelength $\eta(\lambda')$, then

$$(N/V) \cong (4\tau/hc) \int \lambda' I(\lambda') K(\lambda') \eta(\lambda') d\lambda, \tag{4}$$

provided that the light is incident nearly normally on the surface, or at any rate, proceeds nearly normally to the surface after refraction thereat; h and c are Planck's constant and the velocity of light, respectively. In Eq. (4), it is supposed that $K(\lambda')$ is at all wavelengths small in comparison with the radius of the sample, and, further, it is supposed that the terminal state of the transition is empty, so that (N/V) can stand indifferently for the density in the upper state and for the *excess* density in that state.

Other considerations aside, it is desirable to pump at a wavelength as close as possible to that at which the emission occurs, in order to reduce the amount of energy which has to be dissipated (even when $\eta=1$) to the lattice. For CaF_2:Sm^{++}, the most favorable pumping region is the band between 6000 and 6600 A. For (nominal) 0.05% Sm (0.01% Sm^{++}), the absorption constant has around 10 cm^{-1} for an interval of about 500 A in the vicinity of 6400 A (see Fig. 1). Using this figure we can compute, for a particular length and reflectivity, the expected optical maser threshold for pumping in this region. Taking $\lambda=7.08\times10^{-5}$ cm, $\lambda'=6.4\times10^{-5}$ cm, $l=1.2$ cm, $\Delta\nu=1.6$ cm^{-1}, and $R=0.9$, and using the value $\eta=0.2$ corresponding to the efficiency for emission of the 14 118 cm^{-1} line at 20°K (see Sec. A.1), we find 2.5 w cm^{-2}. This, however, is calculated on the assumption that the sample is thin in comparison with $(1/K)$. To get the *average* density throughout the sample up to the required value, we should multiply this by $2Kr$, where r is the radius of the sample; this leads us to approximately 5 w cm^{-2}.

Measurements of the threshold were made with the arrangement shown in Fig. 7, by maintaining constant flash conditions, and progressively reducing the mirror aperture until maser action disappeared. An eosin solution was used to isolate the 16 000-cm^{-1} band. The duration of the pulse was chosen to be long in comparison with the fluorescence decay lifetime. The peak power emitted by the lamp in the wavelength range effective for pumping was then compared with the power emitted in the same wavelength range when the lamp was run continuously at the manufacturer's rating of 1 kw. In one experiment the ratio of the peak flash power to the continuous power was 29. With this peak flash power, maser action disappeared when the mirror aperture was reduced below 0.24 sr. Using the manufacturer's data, we find that the total power emitted within the wavelength range around 16 000 cm^{-1} that can be absorbed by the sample is 23 w when the lamp is run at 1 kw. Assuming the light to be emitted roughly

[8] A. L. Schawlow and C. H. Townes, Phys. Rev. **112**, 1940 (1958).

isotropically, the peak pumping power falling on the sample at threshold is thus about 13 w, which corresponds to an intensity of illumination of about 21 w cm^{-2}. This estimate we believe to be accurate to about a factor of 2. No threshold lower than this was found; some samples showed a threshold that was considerably higher.

It will be seen that the experimental threshold intensity of illumination exceeds that calculated by a factor of 4–8, depending on whether one takes the value expected to lead to the critical density throughout the sample or that giving the critical density only at and close to the surface. Various possible explanations now present themselves. One is that the sample has internal strain, which reduces the Q of the favored modes. Certainly there is evidence for some internal strains from inspection of the crystals between crossed nicols.

A few threshold measurements were made at liquid helium temperatures. Here the measurements had to be made without the eosin filter, because of the necessity of surrounding the Dewar with an outer Dewar containing liquid nitrogen. With the same electrical power, the threshold solid angle appeared to be about a factor of 3 less than in the liquid hydrogen experiment. Since the other bands are now also effective in pumping, and since there are additional reflexion losses at the walls of the outer Dewar, it is difficult to make a quantitative comparison, but it is certainly clear that there is no gross difference between the thresholds at hydrogen and helium temperatures.

3. Experiments at High Illumination Intensities

With the experimental arrangement described in the preceding sections it is possible to explore the optical maser phenomenon over a wide range of pulse durations and of pumping intensities. In this section we shall discuss the dependence of the maser beam intensity on the intensity of illumination and on the previous pumping history.

Figure 8 shows the time dependence of the pumping intensity and of the maser intensity when the sample is illuminated with a pulse having a duration of $\sim 10^{-5}$ sec. The intensity of the pumping flash was chosen to be close to that at which maser action is first seen. The picture shows that maser action begins some 1.5 μsec after the pumping light has passed its peak. Such an effect is to be expected from the nonzero fluorescence lifetime, which implies that a substantial time is required to build up the critical density within the sample. Note too that the maser intensity shown in Fig. 8 is a smoothly varying function of the time; no "spikes" (relaxation oscillations) are to be seen. The time resolution of the circuit and oscilloscope is of the order of 2×10^{-7} sec. The normal fluorescence of the sample, which naturally follows the intensity of the flash lamp, is several orders of magnitude smaller than the stimulated emission and can not be seen in Figs. 8–10.

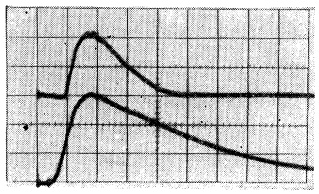

FIG. 9. Optical maser action with a longer light flash. Low-intensity experiment; Upper beam, maser signal; lower beam, pump signal; time scale, 100 μsec per division.

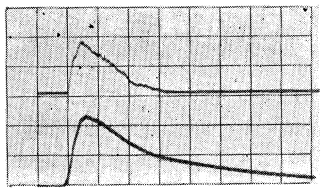

FIG. 10. Repeat of the experiment shown in Fig. 9 with a higher pump intensity, same time scale. The oscilloscope sensitivity was reduced, in comparison with the traces shown in Fig. 9, by five for the maser signal and five for the pump signal.

Figures 9 and 10 show the time dependence of the pumping and maser intensities when the pulse length is $\sim 10^{-3}$ sec. On this time scale the finite pumping time is no longer apparent. However, a new effect is now to be seen. In Fig. 9, in which the pumping intensity never goes far above threshold, the intensity of the pumping light is almost the same at the appearance and extinction points of the maser action. In Fig. 10, however, where the peak pumping intensity is substantially greater, maser action is extinguished long before the pumping intensity has fallen to the value at which maser action began. Thus, at high pumping intensities, the intensity of the maser beam depends not only on the instantaneous value of the pumping intensity, but also on the previous history of the sample.

Output-input curves for a number of flashes are given in Fig. 11. Only points taken in the ascending phase of

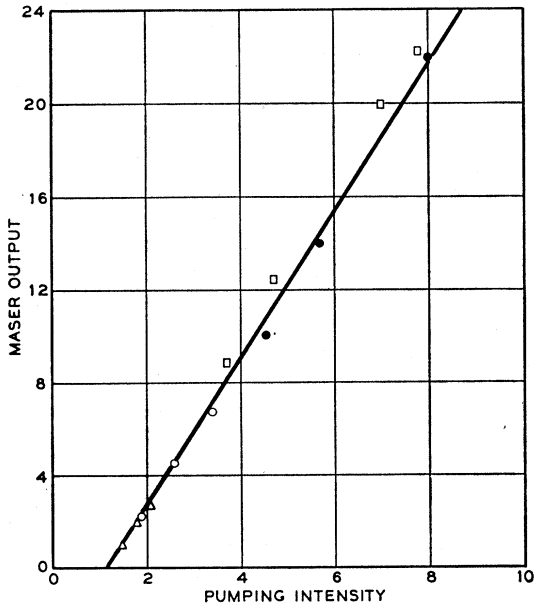

FIG. 11. Plot of maser beam intensity versus pump intensity of illumination. Data from a number of traces are given, but only points from the rising portion of each trace are shown. Points from the descending portions lie low.

the pulse are shown. It will be seen that the maser intensity varies linearly with the difference between the instantaneous pumping intensity and the pumping intensity at threshold, and all the curves coincide. In the falling phase, the maser intensity falls consistently low. This effect, which we associate with heating, will be further discussed in Sec. B.5.

When the ordinary fluorescent light is seen by observation of the light emitted through the sides of the sample, it is found that (with millisecond flashes) the intensity follows fairly closely the intensity of the exciting light. This is not what one would expect. For the elementary theory demands that, once the critical inverted density has been reached, no further increase in the inverted density can occur, and all additional pumping energy (except, of course, for that converted into heat in the course of the radiationless transitions to the upper state) should go into the maser beam. Thus the lateral fluorescence ought to remain independent of time until maser action ceases, and thereafter fall off with the pump intensity. The fact that this is not observed shows clearly that only a small fraction of the excited Sm^{++} atoms are so situated as to contribute to the stimulated emission phenomenon.

4. Photographic Observations

Photographs of the maser beam, using the arrangement described in Sec. B.1, revealed the following facts: (i) The maser beam was generally confined to a range of angle of about $\frac{1}{2}°$; less at excitation levels close to threshold, more at high excitation levels. (ii) The blackened areas on the negatives were not uniformly dark, but consisted instead of a series of spots, randomly arranged, and separated by an average distance of the order of a few tenths of a millimeter. (iii) The same arrangements of spots showed up on all the negatives obtained with a given sample, but the relative intensities depended on the over-all intensity of illumination, the direction of incidence of the exciting light, and the part of the sample most strongly illuminated. Thus, the general effect—the size and shape of the blackened area on the negative—depended on all these factors.

Photographs were also taken with a 10-mm Fabry-Perot etalon interposed in front of the camera lens. One of the resulting pictures is shown in Fig. 12. The effect of interposing the etalon is to permit the passage, in each direction, only of those wavelengths that satisfy the multiple interference condition. As will be seen in Fig. 12, the result is still a collection of dots, but most of the dots now lie on a series of fairly sharp Fabry-Perot rings. From this figure, it will be seen that there are five distinct frequencies in the ring pattern, each having a width rather less than 0.1 cm^{-1}. The limit of resolution of the etalon is approximately 0.03 cm^{-1}. Like the dot pattern, the same ring structure appears in all photographs taken with a given sample.

We offer the following interpretation of these observations. The maser signal consists of at least five discrete frequencies, covering a total range of the order of 0.5 cm^{-1}. Obviously, many modes of the crystal are excited, either consecutively or concurrently; the absence of any "spikes" in the oscilloscope traces would suggest the latter. If the crystal were perfect, one would expect those modes that have frequencies falling within the specified limits to couple to plane waves in the external medium having directions lying on Fabry-Perot rings corresponding to the length of the *sample*; that is to say, one would expect to see rings already in the absence of any external etalon. (Such rings have indeed been observed with highly perfect ruby crystals by Maiman, by Collins and Nelson, and also by the authors.) Evidently, the samples are insufficiently perfect, whether in external dimensions or in homogeneity of refractive index, for this to occur. It is tempting, therefore, to associate the random collection of dots with the individual modes of the sample. The density of modes per steradian in the sample ought to be $2V\nu^2\Delta\nu/c^3$, which for $V=8\times10^{-3}$ cm^3, $\nu=4\times10^{14}$, $\Delta\nu=3\times10^9$ sec^{-1} would be about 3×10^5 sr^{-1}. Allowing for refraction at the end of the sample and for the fact that five distinct frequencies are emitted, we would therefore expect about 2×10^6 "dots" per steradian in the external beam. The density of dots on the negative is about 10^3 cm^{-2}, corresponding to about 2.5×10^6 per steradian. The size of each dot appears to be roughly consistent with the expected diffraction limit of about 5×10^{-4} radian. This interpretation enables one to understand why the dots should appear reproducibly from picture to picture, and also why the intensity associated with each dot should depend on the particular way in which the sample is illuminated; evidently the gain associated with each mode configuration will depend on the distribution of excited atoms through the sample.

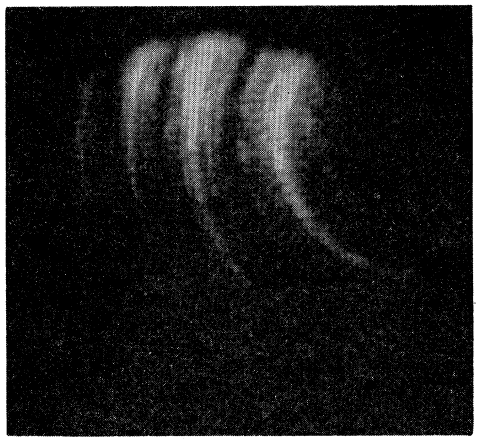

FIG. 12. Photograph of the maser beam taken through a 10-mm etalon with a 500-mm lens.

5. Kinetics of the Maser Effect

We begin by discussing the kinetics of the optical maser effect in the absence of heating effects, and then

extend the discussion to include them. For systems where the density of atoms in the ground state is fixed, and the terminal state empty, the equations governing the system are

$$dN/dt=\gamma I(t)-(N/\tau)(1+\alpha W), \tag{5}$$

$$dW/dt=(\alpha NW/\tau)-\beta W, \quad (N, W>0). \tag{6}$$

Here N stands for the total number of atoms in the upper state, as in Eqs. (3) and (4); $I(t)$ for the time-dependent pumping intensity, W for the number of photons within the crystal associated with the coherent excitation, $\alpha=c\lambda^2/8\pi^3 l r^2\Delta\nu$, $\beta=c(1-R)/l$, and $\gamma=4\pi r^2 lK\lambda'/hc$, and the term $(\alpha NW/\tau)$ represents the stimulated emission process, whereby, for each atom that becomes de-excited, one additional photon appears in the coherent excitation; βW represents the loss of photons in and through the end mirrors. Unit quantum efficiency has been assumed.

Equations (5) and (6) are nonlinear and may under certain circumstances lead to large signal instabilities, as discussed for the microwave maser case.[9] If $I(t)$ becomes time independent, a stable solution may or may not exist. If a stable solution does exist, it will be given by

$$\alpha N=\beta\tau, \tag{7}$$

which is another form of Eq. (3), and

$$W=(\gamma/\beta)I-(1/\alpha), \tag{8}$$

which shows that W (and hence the intensity of the maser beam) should increase linearly with $(I-I_t)$, where I_t is the maser threshold, which in the present notation is $(\beta/\gamma\alpha)$; the linear term is easily seen to correspond to the fact that, for every additional photon absorbed by the sample, one additional photon is emitted into the maser beam.

Where a stable solution, as given by Eqs. (7) and (8), exists, we may linearize Eqs. (5) and (6) and study the approach to the steady-state values for N and W. We set

$$N=(\beta\tau/\alpha)+n, \tag{9}$$

$$W=(\gamma I/\beta)-(1/\alpha)+\omega. \tag{10}$$

Equations (5) and (6) then lead to the following equation for ω:

$$\ddot{\omega}+(I/I_t)(\dot{\omega}/\tau)+(\beta/\tau)[(I/I_t)-1]\omega=0, \tag{11}$$

where $I_t=(\beta/\gamma\alpha)$, the threshold intensity. The solution to this equation is

$$\omega=Ae^{-(\mu-i\nu)t}+Be^{-(\mu+i\nu)t},$$

where $\mu=(I/2I_t\tau)$ and

$$\nu=\{I^2/4I_t^2\tau^2-[(I/I_t)-1](\beta/\tau)\}^{\frac{1}{2}}. \tag{12}$$

In the present experiments, $\tau=2\times10^{-6}$ sec while $\beta=\sim3\times10^9$ sec^{-1}, so that $\beta\tau\gg1$. Thus the response to the sudden application of a step function $I(t)$ should lead to damped oscillatory approach to the steady-state value for ω, provided always that such a steady-state solution exists. The frequency of the damped oscillation should be $\approx(\beta/\tau)^{\frac{1}{2}}$, or $\sim4\times10^7$ sec^{-1} in the present case; the damping time should be $\approx\tau$. These oscillations, if they occur, lie beyond the limit of frequency response of our measuring instruments.

We turn lastly to the "heating" effect reported in Sec. B.3. Plainly there are various sorts of heating effect which might be occurring. In particular, we may distinguish: (i) Accumulation of Sm^{++} atoms in the final state of the maser transition, which makes the "temperature" defined between the terminal state and the ground state rise progressively with time. (ii) Accumulation of Sm^{++} atoms in some state intermediate between the terminal state and the ground state. This in effect progressively exhausts the ground state to the point at which no further pumping can be achieved. (iii) Heating of the whole system (samarium atoms plus lattice), leading, among other things, to an increased fluorescence linewidth and so to an increased threshold.

Each of these effects will lead to a decrease in maser beam intensity—or an increase in the apparent threshold, which is the same thing—proportional to the total amount of pumping which has occurred, which is $\int Idt$. Careful comparison of the extension of curves shown in Fig. 10 into the region of the falling part of the pulse with the measured time dependence of the pumping intensity show in fact that the maser intensity may be described by the equation:

$$\beta W=a[I-I_t-(\tau')^{-1}\int Idt], \tag{13}$$

where τ', for one particular experiment, was approximately 10^{-3} sec. Now this time is clearly far too long for explanation (i) above to be correct; for it is easily shown that this mechanism ought to lead to $\tau'\sim\tau$. With regard to mechanism (ii), we note that the threshold intensity corresponds to a pumping rate of about 8×10^{20} atoms cm^{-3} sec^{-1}, compared with a total Sm^{++} content of 1×10^{18} cm^{-3}; thus we would expect $\tau'\sim1.3\times10^{-3}$ sec, which is very much of the order found. However, explanation (iii) leads, under adiabatic conditions, to $(\tau')^{-1}\sim(\zeta I_t/C_p r)[(1/\Delta\nu)d\Delta\nu/dT]$, where ζ is the fraction of the light going into heat, C_p the specific heat per unit volume, r the radius of the sample, and $\Delta\nu$, as before, the fluorescence linewidth. Substituting $\Delta\nu_0=1.6$ cm^{-1}, $d\Delta\nu_0/dT=0.2$ cm^{-1} deg^{-1}, $C_p=1.6\times10^{-2}$ joule deg^{-1} cm^{-3}, $\zeta=0.3$, $r=0.1$ cm, and $I_t=20$ w cm^{-2}, we obtain $\tau'\sim10^{-3}$ sec, which again is of the order of magnitude found. Thus, on the basis of τ' alone, we are unable to distinguish between mechanisms (ii) and (iii).

[9] H. Statz and G. de Mars, in *Quantum Electronics*, edited by C. H. Townes (Columbia University Press, New York, 1960).

To investigate the matter further, we made a few measurements with an intensity of illumination in the range 10–30 w cm^{-2} with pulses lasting up to 1 sec. We found that, for intensities below about 15 w cm^{-2}, the temperature of the sample (whether measured spectroscopically, by observation of the 14 497-cm^{-1} absorption line, or by means of a thermocouple attached to the sample) remained at or close to 20°K. For intensities greater than this, the sample became thermally disconnected from the bath, and the sample temperature rose within 1 sec to a value greater than 100°K. Furthermore, absorption measurements within the 16 000-cm^{-1} band gave no evidence for ground-state depopulation. The authors therefore believe that explanation (iii) above is correct, and that there is no evidence at the present time for accumulation in any level between the terminal state and the ground state. This is in any case reasonable on other grounds. The energy difference between the terminal and ground states is equal, within a factor of 1.5, to the principal reststrahlen energy at 242 cm^{-1},[10] so that rapid nonradiative depopulation ought to occur.

[10] F. Matossi and H. Brix, Z. Physik **92**, 303 (1934).

SUMMARY AND ACKNOWLEDGMENTS

The work reported in this paper has served further to elucidate the level scheme for $CaF_2:Sm^{++}$ and to demonstrate optical maser effects in this material. The spectroscopic analysis is as yet incomplete because of our inability to make firm term assignments. The maser experiments have shown that the threshold intensity of illumination is about an order of magnitude higher than anticipated by the Schawlow-Townes theory, and also that, even close to threshold, many modes (of the order of 10^3) are excited instead of just one. At the present time, it is not clear whether these facts are related, and likewise it is not clear how much the situation would be improved if samples optically more nearly perfect were available.

The authors have greatly profited from the work of W. L. Bond, who developed the techniques for preparing the samples for optical maser observations. They are also indebted to H. G. Guggenheim for his continuous effort to prepare and improve the quality of the crystals used in this investigation. It is a great pleasure to thank for their technical assistance during various parts of the work J. Ditzenberger, R. H. Kaiser, B. Prescott, and M. Simms.

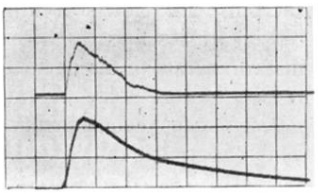

FIG. 10. Repeat of the experiment shown in Fig. 9 with a higher pump intensity, same time scale. The oscilloscope sensitivity was reduced, in comparison with the traces shown in Fig. 9, by five for the maser signal and five for the pump signal.

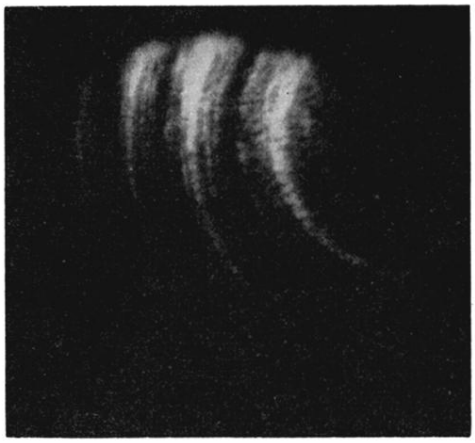

FIG. 12. Photograph of the maser beam taken through a 10-mm etalon with a 500-mm lens.

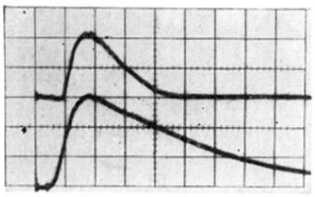

FIG. 9. Optical maser action with a longer light flash. Low-intensity experiment; Upper beam, maser signal; lower beam, pump signal; time scale, 100 μsec per division.